ELSEVIER

March 1996

Optical Materials 5 (1996) 159–167

OPTICAL Materials

# Concentration quenching in erbium implanted alkali silicate glasses

E. Snoeks, P.G. Kik, A. Polman

*FOM Institute for Atomic and Molecular Physics Kruislaan 407, 1098 SJ Amsterdam, The Netherlands*

Received 18 April 1995; accepted 27 October 1995

**Abstract**

A comparison is made of photoluminescence properties of six sodalime and alkali-borosilicate glasses implanted with Er to concentrations as high as $1.4 \times 10^{21}$ at./cm$^3$. Clear photoluminescence (PL) spectra around 1.54 μm, due to the $^4I_{13/2} \rightarrow {}^4I_{15/2}$ transition in $Er^{3+}$ are observed, of which the shape depends on the host glass composition. PL lifetimes in the range of 0.9–12.6 ms are found, depending on glass and Er concentration. In borosilicate glass, implantation-induced defects remain after annealing and cause quenching of the Er luminescence due to a direct coupling to the Er. Such defects are not present in Er-implanted sodalime glass after annealing. In both types of glass the luminescence lifetime decreases strongly with concentration due to a concentration quenching effect in which energy migration takes place due to energy transfer between Er ions, followed by quenching at hydroxyl groups. Concentration quenching via this mechanism is less strong in the borosilicates than in the sodalime glasses, but because of the quenching effect of implantation-induced defects in borosilicates these glasses are not suitable for optical doping by ion implantation.

## 1. Introduction

Erbium-doped materials have recently become of great interest because of their use as an optical gain medium [1]. Trivalent Er shows an optical transition (intra-4*f*) around 1.54 μm, a standard wavelength in silica-based optical fiber communication systems. Erbium-doped fiber amplifiers operating around 1.54 μm are now commercially available, and a need has arisen for *planar* amplifiers that can be integrated with planar optical devices such as optical splitters, switches, and multiplexers [2]. Sodium containing silicate glasses are suitable substrates for these applications, because fiber compatible waveguides can be fabricated using a simple ion-exchange process, where $Na^+$ from the glass is replaced by ions that raise the refractive index, such as $K^+$ or $Ag^+$ [3–5].

To achieve sufficient gain in a few centimeters, as opposed to the meters used for Er-doped fiber amplifiers, the Er concentration needs to be on the order of an atomic percent. Ion implantation can be used to incorporate such high concentrations with well-controlled doping profiles in the center of an optical waveguide, where the pump intensity is high. In this way, population inversion between the first excited and the ground state can be achieved if the luminescence lifetime is sufficiently long. However, high concentrations can give rise to undesirable effects like concentration quenching and cooperative upconversion [6–8], which reduce the lifetime.


*SSDI* 00925-3467(95)00063-1

This article will focus on concentration quenching, resulting from interaction between excited and unexcited Er ions. Due to this interaction, energy can migrate through the glass until a quenching center is met and the excitation is lost. The efficiency of this process depends on the mean Er–Er distance, the energy exchange rate, and the density of quenching sites. In this article, a comparison is made of photoluminescence properties of six different Er implanted sodalime silicates and alkali-borosilicate glasses, with the aim to find the glass with the lowest luminescence quenching. This glass may then be used to design a planar optical amplifier operating at 1.54 μm.

The experiments show two types of Er-fluence dependent luminescence quenching: (a) concentration quenching due to energy migration at high Er concentration followed by de-excitation at a quenching site (hydroxyl groups), (b) an additional effect only observed in alkali-borosilicate glass, namely quenching by direct coupling of Er ions to implantation-induced defects in the glass.

Table 1
Compositions of the used silicates in at.%. The question marks indicate that B cannot be detected with RBS

| | FP [a] | Pilk [b] | Ca-rich [c] | BGG 31 [d] | Pyrex [e] | CRN 0211 [f] |
|---|---|---|---|---|---|---|
| Si | 25.6 | 25.0 | 24.6 | 17.6 | 25.4 | 22.4 |
| Na | 9.8 | 11.5 | 6.5 | 6.8 | 2.5 | 4.7 |
| Ca | 2.4 | 3.0 | 7.0 | - | - | - |
| K | 0.6 | - | - | < 0.01 | 0.2 | 3.1 |
| Al | 0.5 | - | - | 7.1 | 0.9 | 0.8 |
| B | - | ? | ? | 6.0 | 7.0 | 5.3 |
| Mg | 0.6 | - | - | - | - | - |
| Fe | < 0.01 | - | - | - | - | - |
| Ti | - | - | < 0.4 | - | - | 0.8 |
| Zn | - | - | 1.0 | - | - | 1.8 |
| As | - | - | - | 0.06 | - | - |
| F | - | - | - | 4.2 | - | - |
| O | 60.4 | 60.3 | 60.1 | 58.3 | 64.0 | 61.2 |

[a] Fisher Premium sodalime silicate, Ref. [4].
[b] Pilkington sodalime silicate, from RBS data.
[c] Ca-rich sodalime silicate, from RBS data.
[d] Integrierte Optik-Technologie alkali-borosilicate, Ref. [5].
[e] Pyrex 7740 alkali-borosilicate (Corning), Ref. [9].
[f] Corning 0211 alkali-borosilicate, Ref. [4].

## 2. Experimental

In this study, six commercially available silicate glasses were investigated: three different sodalime glasses (Fisher Premium, Pilkington, and a Ca-rich sodalime glass), and three different sodium containing borosilicates (IOT-BGG 31, Corning 0211, and Pyrex). The glass compositions, which are tabulated in Table 1, are taken from the literature [4,5,9], except for the Ca-rich sodalime and Pilkington sodalime silicates. For the latter two, compositions were determined using Rutherford backscattering spectrometry (RBS) [10], because the specifications were not available. As can be seen in Table 1, all glasses contain Na at different concentrations as the most important network modifying cation, and B is found in BGG 31, Pyrex, and Corning 0211. Note that $B_2O_3$ is a network former, like $SiO_2$. The concentration of hydroxyl groups (–OH) in all six glasses was estimated using infrared (IR) transmission and reflection measurements between 2000–4000 $cm^{-1}$ (2.5–5.0 μm), using a Perkin-Elmer 811 IR spectrometer.

All six glasses were implanted with 400 or 500 keV Er ions at room temperature. The ion current density on sample was ~0.5 $\mu A/cm^2$, and the implanted fluences ranged from $8.6 \times 10^{14}$ to $1.8 \times 10^{16}/cm^2$, corresponding to Er peak concentrations up to 2.0 at.%. RBS measurements show that the Er concentration depth-profiles are Gaussian shaped, with a mean depth of ~100 nm, and a full width at half maximum of ~100 nm. To avoid electrical charging of the glasses during ion irradiation, a 420 Å Al film was evaporated on the glass surface. It was etched off in a NaOH solution after implantation. Thermal annealing was performed in a tube-furnace at a base pressure below $5 \times 10^{-7}$ mbar, at temperature up to 600°C. All anneals were done for one hour.

Photoluminescence (PL) spectroscopy was carried out at room temperature, with the 514.5 nm or the 488.0 nm line of an Ar-ion laser as excitation source. Powers of 350 mW were used in a ~0.3 mm diameter spot, for which no beam heating of the samples was observed. The luminescence signal was spectrally analysed with a 48-cm monochromator, and detected with a liquid-nitrogen-cooled Ge detector, yielding a spectral resolution of 2.3 nm. The pump beam was chopped at 12 Hz and spectra were

recorded using a lock-in amplifier. Time-resolved luminescence decay measurements were performed using a 1.5 ms, 1.4 W pump pulse with a cutoff time shorter than 150 μs, and averaged using a digital oscilloscope.

## 3. Results and discussion

### 3.1. Photoluminescence

First, we will compare the six different silicate glasses implanted with Er to a fixed peak concentration of 0.2 at.%. All samples were annealed to obtain maximum PL intensity and lifetime. The annealing temperature dependence of the PL intensity in each examined glass was qualitatively the same as shown in Ref. [11] for Fisher Premium sodalime. The maximum PL intensity was reached after annealing above 500°C, except for BGG 31 where 400°C was sufficient, and Pyrex where 600°C was required.

Fig. 1 shows the PL spectra of the Er-implanted samples, normalized to integrated signal. All samples show broad PL spectra around 1.54 μm, characteristic for the $^4I_{13/2} \rightarrow {}^4I_{15/2}$ intra-4$f$ transition of $Er^{3+}$ [12]. The spectra in BGG 31 and Pyrex are clearly broader than the spectra in the other hosts. This is ascribed to the relatively low concentration of network modifiers (Na, Ca, K, Mg) in these glasses in addition to the presence of B (a network former). This leads to a more inhomogeneous distribution of Er sites, leading to more inhomogeneous broadening of the spectra.

The PL lifetimes ($\tau$) measured at 1.535 μm after annealing are indicated in the top left-hand corners of Figs. 1a–f. As can be seen, the PL lifetime depends strongly on host material: 12.6 ms is measured in the Ca-rich sodalime glass, and only 0.9 ms in Pyrex. The measured PL decay rate is the sum of radiative and non-radiative decay rates. Our earlier work has shown that the radiative decay rate of Er implanted in sodalime glass is $W_r = 45\ s^{-1}$ (corresponding to 22 ms), independent of Er concentration and annealing treatment [11,13]. Because of the shielding of the 4$f$ electrons by the outer lying $5s^25p^6$ shells [12], it can be assumed that the radiative decay rate in similar multicomponent silica-based materials is approximately the same. Therefore, the observed strong variation of PL lifetime with host is ascribed to relatively large differences in non-radiative decay rate, as will be discussed hereafter.

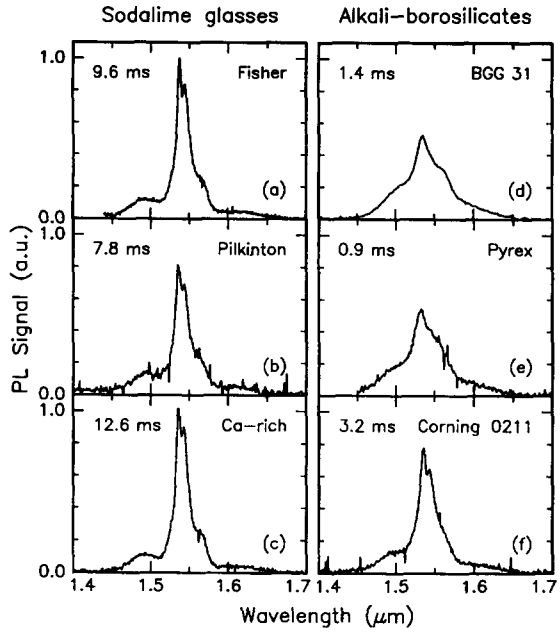


Fig. 1. Room temperature PL spectra of six different Er-implanted sodium containing silicate glasses: Fisher Premium (a), Pilkington (b), and Ca-rich (c) are sodalime glasses; BGG 31 (d), Pyrex (e), and Corning 0211 (f) are alkali-borosilicates. The Er concentration was 0.2 at.% in each case, and the PL lifetimes at 1.535 μm are indicated in the figures. All samples were annealed at 400-600°C.

### 3.2. Hydroxyl impurities

Fig. 2 shows IR-absorption spectra in the range from 2200 to 4000 $cm^{-1}$ for all the six unimplanted glasses. The strong absorption below 2400 $cm^{-1}$ is due to excitation of Si–O vibrations [9,14]. For the borosilicates (Figs. 2d–f) three clear absorption bands at 2500, 2700, and 3600 $cm^{-1}$ are visible. The bands at 2700 and 3600 $cm^{-1}$ are also seen in the three sodalime glasses (Figs. 2a–c), but much weaker. All bands are ascribed to absorption by hydroxyl groups, and in particular the 3600 $cm^{-1}$ (2.8 μm) band is due to the stretch vibration of free –OH [9,14,15]. Using an absorption cross section of $1.2 \times 10^{-19}$ $cm^2$ for this band [16], an estimate of the density of free –OH ($N_{OH}$) can be made from the measured

absorption coefficient at 3600 $cm^{-1}$. The results of these estimates are indicated in Fig. 2 for each glass in units of $-OH/cm^3$. The –OH concentrations range from $0.8 \times 10^{19}$ at./$cm^3$ in Fisher Premium soda-lime glass to $3.9 \times 10^{19}$ at./$cm^3$ in Pyrex.

It is known that free –OH is one of the important quenching centers in Er-doped glasses [17–19]. The energy of the $^4I_{13/2} \rightarrow {}^4I_{15/2}$ transition in $Er^{3+}$ ($\sim$ 6500 $cm^{-1}$) corresponds to the energy of the second harmonic of the –OH stretching vibration. Therefore, if an $Er^{3+}$ ion is coupled to –OH, non-radiative relaxation of the $^4I_{13/2}$ $Er^{3+}$ level can occur by excitation of two –OH vibrational quanta.

Fig. 3 shows the Er PL decay rate (i.e. $1/\tau$) plotted against the density of free –OH in the six glasses, using the data depicted in Figs. 1 and 2. Although the data show a trend relating the measured Er PL lifetimes in the various glasses to the estimated density of free –OH, no clear correlation is found. This will be discussed in detail further on,

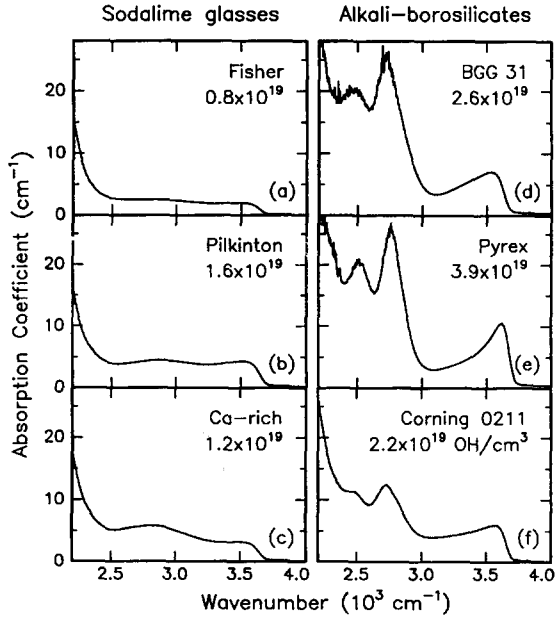


Fig. 2. Infrared absorption spectra in each of the unimplanted glasses: Fisher Premium (a), Pilkington (b), and Ca-rich sodalime (c); BGG 31 (d), Pyrex (e), and Corning 0211 (f). The OH densities given in the figure for each glass in units of $-OH/cm^3$ are calculated using an absorption cross section of $1.2 \times 10^{-19}$ $cm^2$.

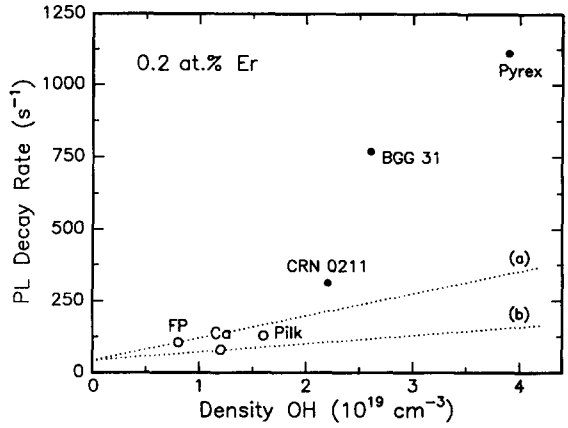


Fig. 3. Correlation between the PL decay rate of the six different Er-implanted (400 or 500 keV, $1.4 \times 10^{20}$ $Er/cm^3$) silicate glasses (after annealing), and the density of free –OH in these glasses. Circles are used for sodalime glasses, and black dots for alkali-borosilicates. The dotted lines are calculated with Eq. (1), using $W_r = 42\ s^{-1}$, $N_{Er} = 1.4 \times 10^{20}$ at./$cm^3$, and either $C_{Er,Er} = 2.3 \times 10^{-51}$ $m^6/s$ (a) or $0.86 \times 10^{-51}$ $m^6/s$ (b).

using additional data on the Er-concentration dependence of the PL lifetimes.

### 3.3. Concentration quenching and defects

In two glasses – Fisher Premium as an example of a sodalime glass, and BGG 31 to represent the alkali-borosilicates – the Er implant fluence was varied up to $1.8 \times 10^{16}$ $Er/cm^2$ (peak concentration of 2.0 at.%). Photoluminescence decay rates were measured at room temperature after annealing.

#### 3.3.1. Sodalime glass

The dots in Fig. 4 show the PL decay rate (i.e. $1/\tau$) of Er in Fisher Premium sodalime glass as a function of Er concentration (the atomic density at the peak of the Gaussian implantation profile), after annealing at 512°C. The data show that the PL decay rate increases almost linearly with Er density.

This concentration quenching effect and the role of defects and impurities can be understood from Fig. 5, which shows a schematic picture of the three ways how an excited Er ion can de-excite: (i) by emission of a photon (wavy arrow), (ii) by non-radiative relaxation through coupling to a quenching site (for instance –OH), or (iii) by energy transfer to a neighboring Er ion (straight lines) [20]. In the latter

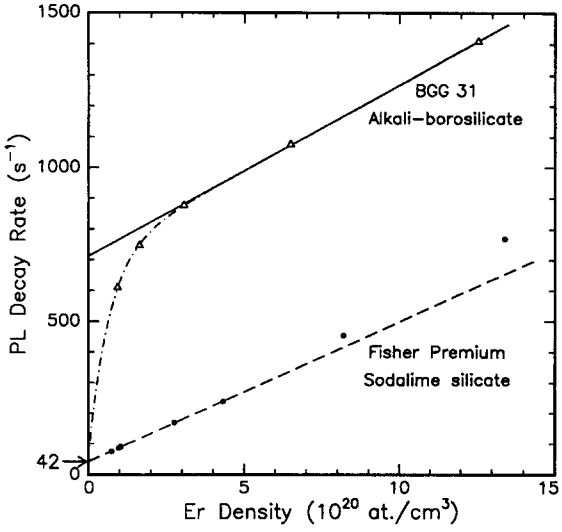


Fig. 4. Erbium photoluminescence decay rate versus Er peak density (after annealing). The dots show data for Er in Fisher Premium sodalime glass. The dashed line is a linear fit through the data below $5\times10^{20}$ Er/cm$^3$, and intercepts the $y$-axis at 42 s$^{-1}$. The triangles show data for Er implanted BGG 31 alkali-borosilicate glass after annealing. The solid line is a linear fit through the data above $2\times10^{20}$ Er/cm$^3$, and the ··· line is a fit based on a model which includes the effect of irradiation damage.

way the excitation can migrate through the glass, and when an Er ion is met which is coupled to an –OH group the excitation is lost.

For a homogeneous distribution of Er ions, and a low density of quenching sites, and assuming that the energy exchange between Er ions takes place via dipole–dipole interaction, the total concentration-dependent decay rate is given by [8,21–23]

$$W = W_r + W_i + 8\pi C_{Er,Er} N_q N_{Er}. \quad (1)$$

Here $W_r$ is the radiative decay rate, $W_i$ is the internal non-radiative quench rate, $C_{Er,Er}$ is an Er–Er interaction constant [8], and $N_q$ and $N_{Er}$ are the density of quenching sites and Er ions, respectively. Note that $W_r + W_i$ is the decay rate in absence of migration. It is assumed in Eq. (1) that the absorption spectrum of a quenching site is identical to the absorption spectrum of an $Er^{3+}$ ion in sodalime glass. This simplification may be made in the case that the quenching mechanism is via excitation of vibrations in –OH closely bound to a limited number of Er ions.

Eq. (1) is used to fit the data for Er in sodalime glass in Fig. 4. Below $5\times10^{20}$ at./cm$^3$ excellent agreement is achieved: the dashed line is the result of a linear fit with a slope of $(4.6\pm0.4)\times10^{-25}$ m$^3$/s. The extrapolated PL decay rate for zero Er density is $41.9\pm1.1$ s$^{-1}$. This value is very close to the experimental value of the radiative decay rate $W_r = 45$ s$^{-1}$ which we found in an earlier independent experiment [13]. This implies that the internal

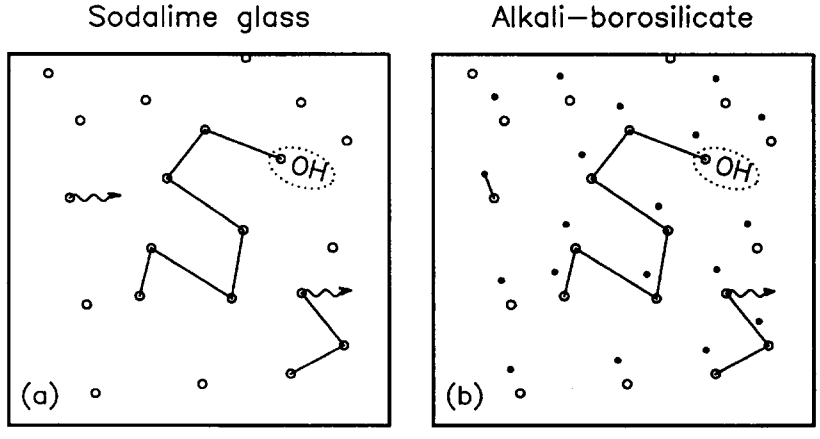


Fig. 5. Schematic representations of the possible luminescence decay mechanisms in Er-implanted silica glass. (a) After excitation, each Er ion (circle) has a probability to emit a photon (wavy arrow), or to transfer the excitation to a neighboring Er ion (straight line). Rapid quenching takes place at a small fraction of Er ions that are closely bound to an –OH group. In (b), a third decay mechanism is added; the probability for each Er ion to directly loose the excitation to an implantation-induced defect (black dot). As is discussed in the text, (a) corresponds to Er-implanted sodalime glass, while (b) refers to effects in Er-implanted borosilicate glass.

non-radiative decay rate $W_i \approx 0$ [1], which means that in absence of quenching due to migration all Er ions (except those coupled to –OH) decay in a purely radiative fashion. The data in Fig. 4 can be described assuming a constant density of quenching centers $N_q$, which implies that this density is independent of Er fluence, and therefore these quenchers are *not* related to the damage created by the ion beam.

To supply support for the latter conclusion, samples were prepared in which irradiation damage was provided independently from the Er concentration in the following way. A sample was first implanted with a low fluence of Er at 500 keV ($1.4 \times 10^{15}$ Er/cm$^2$, corresponding to $1.0 \times 10^{20}$ Er/cm$^3$), and subsequently irradiated with 1.8 MeV Au to fluences in the $1 \times 10^{14}$–$1 \times 10^{16}$ Au/cm$^2$ range. The projected range of the Au ions is well beyond the Er profile, so that ion irradiation damage is provided all through the Er-doped region [2], without changing the chemical environment of the Er. All samples were annealed at 512°C after the irradiations were completed. The crosses (×) in Fig. 6 show the Er PL decay rate of the Au co-irradiated sample as a function of total irradiation fluence (Er + Au). As can be seen, the PL decay rate remains almost constant with Au fluence. For comparison, Fig. 6 also includes the Er PL decay rate as a function of fluence in the case that only 500 keV Er is implanted (filled data, points, same data as in Fig. 4). As the additional Au fluence, which produces a similar amount of irradiation damage per ion as the Er [24], does not cause a large increase in the Er PL decay rate, it is confirmed that the strong increase of PL decay rate with increasing Er fluence is *not* explained by accumulation of beam-induced damage, but by an Er concentration quenching effect, i.e. migration followed by quenching at a fixed density of quenching sites.

If it is assumed that all free –OH contributes to quenching, then $N_q = N_{OH} = 8 \times 10^{18}$/cm$^3$ (as estimated in Section 3.2) can be inserted in Eq. (1). From the slope of the fit, $C_{Er,Er} = 2.3 \times 10^{-51}$ m$^3$/s is then extracted. This implies that for an Er concentration of approximately $\sim 3 \times 10^{18}$ Er/cm$^3$ the Er–Er energy transfer rate equals the radiative decay rate. The value for $C_{Er,Er}$ will be compared with other data in Section 4.

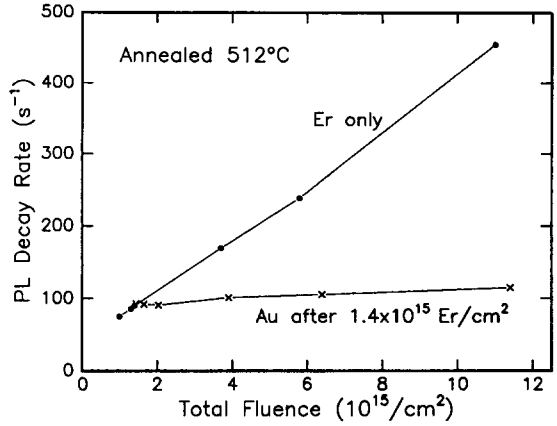


Fig. 6. Erbium PL decay rates in sodalime glass as a function of total implanted fluence, after annealing. The solid data points show the Er PL decay rate when only 500 keV Er is implanted. The crosses (×) show the Er decay rate in a sample first implanted with $1.4 \times 10^{15}$ Er/cm$^2$ and subsequently with 1.8 MeV Au to fluences ranging from $1 \times 10^{14}$ to $1 \times 10^{16}$ Au/cm$^2$. All samples were annealed at 512°C after all irradiations were completed.

A final detail observed in Fig. 4 is that for Er densities above $5 \times 10^{20}$ at./cm$^3$ the measured PL decay rates in sodalime glass deviate from the linear behavior predicted by Eq. (1). This effect may be related to the fact that at high fluence ion irradiation the high density of displaced atoms can cause local non-uniformities in the Er concentration. This then would enhance concentration quenching. Microscopic redistribution of impurities in ion irradiated $SiO_2$ has been observed before; for instance, Ag [25] or Au [26] coalesce into metallic nano-clusters, and metals such as Fe [27] can form oxide clusters in silica when sufficient mobility is provided by an ion beam.

### 3.3.2. Alkali-borosilicate glass

The triangles in Fig. 4 show the measured PL decay rate of Er implanted BGG 31 alkali-borosilicate glass as a function of Er density after annealing at 400°C. The used Er fluences range from 0.09 to

[1] Using $W_r = 45$ s$^{-1}$, $W_i$ would be $-3$ s$^{-1}$, which is unphysical, and possibly related to the fact that the linear behavior in Eq. (1) is only valid when the density of quenching sites is low compared to the density of Er, which is not the case in the limit $E_{Er} \to 0$.

[2] The nuclear energy loss per ion of both Er and Au averaged in the Er-doped region is 300 eV/Å and the electronic energy loss 30 and 140 eV/Å, respectively [Monte Carlo simulation TRIM'89 [24]].

$1.2 \times 10^{16}$ ions/cm$^2$. For all concentrations, the decay rate is higher than what is found for Er implanted sodalime glass. As can be seen, above $3 \times 10^{20}$ Er/cm$^3$, the PL decay rate depends linearly on the Er density. Below $3 \times 10^{20}$ Er/cm$^3$ the decay rate is a steeper function of Er density than above $3 \times 10^{20}$ Er/cm$^3$. This behavior is clearly different from what is observed in sodalime glass. The high dose data for Er implanted BGG 31 can be described using Eq. (1). A slope of $(5.6 \pm 0.5) \times 10^{-25}$ m$^3$/s and $W_0 = 718 \pm 2$ s$^{-1}$ are found. However, this model which assumes a constant number of sinks ($N_q$) and a constant $W_i$, does not explain the low fluence data.

We suggest that for the case of BGG 31, ion implantation induced defects, of which the density is Er-fluence dependent, play a role in the quenching of the Er luminescence. Therefore a modification in the concentration quenching model has to be made to account for beam induced effects. $C_{Er,Er}$ and $W_r$ are independent of Er fluence. The parameters $N_q$ and $W_i$ in Eq. (1), however, may possibly increase (decrease is very unlikely) with Er fluence. Let us first consider that $N_q$ – which is the density of quenching centers that couples only to a small fraction of the Er ions – would increase during ion irradiation due to the formation of beam-induced defects. According to Eq. (1), the slope in Fig. 4 would then *increase* with Er density (fluence). The low-fluence data, however, show a *decrease* of the slope, and therefore cannot be explained by an increase in $N_q$. The other possibility is that $W_i$ increases with Er fluence, i.e. an increase in the internal quench rate of each Er ion with increasing fluence $\phi$. This means that Er ions directly couple to irradiation induced defects, and all Er ions have a certain probability to lose the excitation to such a defect. This is schematically indicated in Fig. 5b, where the black dots represent beam-induced defects. Using a damage creation model – in which the density of irradiation induced defects follows an exponentially saturating law proportional to $[1 - \exp(-\phi/\phi_c)]$ [28], with $\phi_c$ a characteristic fluence – $W_i$ can be written as a function of Er fluence:

$$W_i(\phi) = [W_{sat} - W_r - W_i(0)]\,[1 - \exp(-\phi/\phi_c)] + W_i(0). \quad (2)$$

Here $W_{sat}$ is the Er PL decay rate in absence of energy migration when irradiation damage has saturated, and $W_i(0)$ the internal quench rate before irradiation damage is done.

The -·- line in Fig. 4 shows the result of a fit using Eqs. (1) and (2). The fit describes the data very well. The fit parameters are: $\phi_c = (6.8 \pm 0.4) \times 10^{14}$ Er/cm$^2$, $8\pi C_{Er,Er} N_q = (5.6 \pm 0.5) \times 10^{-25}$ m$^3$/s, and $W_{sat} = 715 \pm 3$ s$^{-1}$. The intercept with the $y$-axis ($W_r + W_i(0)$) could not be determined accurately due to the fact that no PL lifetime data were available for very low Er fluences. These data imply that in the absence of excitation migration, Er ions decay by both radiative decay and non-radiative decay due to coupling to irradiation-induced defects. Using the concentration of free –OH in BGG 31, $N_q = 2.6 \times 10^{19}$/cm$^3$ (see Section 3.2), we find $C_{Er,Er} = 8.6 \times 10^{-52}$ m$^6$/s from the fit results. This value for $C_{Er,Er}$ is lower than in the case of Er in Fisher Premium sodalime glass, which will be discussed in Section 4.

The effect of ion irradiation damage on the Er luminescence lifetime which is observed in BGG 31 alkali-borosilicate glass, and not in sodalime glass, is attributed to the presence of boron in the network. Electron-spin-resonance (ESR) studies have shown that B enhances the irradiation sensitivity for electronic damage in silica by orders of magnitude, due to formation of B-related point defects [29]. The suggestion that B enhances Er PL quenching is supported by Fig. 3, where it can be seen that all three Er-implanted alkali borosilicates (black dots) show significantly higher PL decay rates than the sodalime glasses (circles). To illustrate this the dotted line (a) is drawn in Fig. 3 which show the PL decay rate as a function of OH density according to Eq. (1) with $C_{Er,Er} = 2.3 \times 10^{-51}$ m$^6$/s found for Er in Fisher Premium sodalime glass. A similar line, but then using the value $C_{Er,Er} = 0.86 \times 10^{-51}$ m$^6$/s as found for Er in BGG 31 alkali-borosilicate is also shown [dotted line (b)]. As can be seen, neither of these lines describe the high decay rates found experimentally for the borosilicate glasses, indicating that additional irradiation induced damage plays a role in these borosilicates.

## 4. Comparison to other work

In the previous section it was found that the excitation transfer constant ($C_{Er,Er}$) in Fisher soda-

lime glass is $2.3 \times 10^{-51}$ m$^6$/s, and in BGG 31 alkali-borosilicate glass $0.86 \times 10^{-51}$ m$^6$/s. The difference can be explained to some extent by the fact that due to inhomogeneous broadening, the Er PL spectrum in alkali-borosilicate glass is broader than in sodalime glass (Fig. 1). Therefore, the mean overlap integral of the emission and absorption spectrum between nearest neighbors is smaller in BGG 31 than in sodalime, or put differently, the effective distance between well matching Er ions becomes larger. Also, differences in the phonon spectra of the glasses may cause differences in transfer rate. The values of $C_{\mathrm{Er,Er}}$ found here are in the same range as values found by Gapontsev et al. ($0.7 \times 10^{-51}$ m$^6$/s) by varying the –OH concentration in phosphate glass samples with fixed Er density [17,30].

The results presented in this article concern the energy transfer between excited and non-excited Er ions, which leads to lowering of the PL decay time when a small fraction of Er ions is excited. However, in an actual Er-doped optical amplifier, where a high fraction of excited Er ions is needed, a second quenching mechanism becomes important: *cooperative upconversion.* In this process, energy is transferred between two *excited* Er ions, leaving one of both ions de-excited [6–8]. In an earlier publication we showed that the de-excitation rate of Er in sodalime glass at a concentration of 0.2 at.% ($\approx 1.4 \times 10^{20}$ at./cm$^3$) can increase four-fold due to upconversion [31]. The upconversion coefficient is highest in glasses in which Er shows broad PL spectra, because the upconversion process is resonant only in the long wavelength part of the transition [31]. Therefore we predict that glasses such as BGG 31 and Pyrex in which $Er^{3+}$ shows broad PL spectra (see Fig. 1), will suffer from relatively strong cooperative upconversion, whereas the sodalime glasses with the narrower spectra will show less upconversion.

The $4f$ levels are relatively fixed, because they are electronically shielded by outer lying $5s^25p^6$ shells [12]. Therefore, neither energy migration, nor cooperative upconversion can be completely avoided by choice of host. The final choice should be made by comparing the effects of migration-quenching and upconversion-quenching. In an Er-based optical amplifier operating at 1.54 μm, the rate of de-excitation is found by solving the rate equation for the fraction $n$ of excited Er ions: $\mathrm{d}n/\mathrm{d}t = -n/\tau - CN_{\mathrm{Er}}n^2$, where $C$ is the upconversion coefficient. In the limit $n \to 0$, the 'spontaneous' de-excitation rate is given by $1/\tau$, and in the limit $n \to 1$ by the sum $1/\tau + CN_{\mathrm{Er}}$. In sodalime glass, $C = 3 \times 10^{-24}$ m$^3$/s [31], and for Er concentrations above $1.5 \times 10^{19}$ at./cm$^3$ ($\sim 0.02$ at.%) $CN_{\mathrm{Er}} > 1/\tau$, i.e. upconversion is the dominant de-excitation mechanism. For planar amplifiers, where concentrations are usually higher than $1.5 \times 10^{19}$ at./cm$^3$, the most suitable host is therefore the host which shows least upconversion, i.e. narrowest PL spectrum. From the point of view of Er luminescence properties, the three sodalime glasses which were examined in this article are equally well suited. When upconversion is not the dominant decay mechanism, for instance in fiber amplifiers, broad PL spectra (as for instance in borosilicates) are more preferred. However, for the borosilicates, ion implantation is not a suitable technique for optical doping due to the effect of implantation-induced damage on the Er luminescence lifetime.

## 5. Conclusions

Six different silicate glasses (three sodalime glasses and three alkali-borosilicates) were implanted with Er and annealed. For each glass, the PL spectrum around 1.54 μm, the PL lifetime, and the concentration of free –OH were measured. The PL lifetime depends strongly on host glass. This is attributed to differences in non-radiative decay rates; –OH is one of the quenching sites. For two glasses the Er concentration (implant fluence) was varied in the range of $7 \times 10^{19}$–$1.5 \times 10^{21}$ at./cm$^3$. In both cases the PL decay rate increases with Er density.

(a) Sodalime glass. The increase in PL decay rate with Er density is described using a simple concentration quenching model with energy migration due to Er–Er interactions as rate-limiting process. The Er–Er energy transfer coefficient $C_{\mathrm{Er,Er}} = 2.3 \times 10^{-51}$ m$^6$/s. After annealing, implantation-induced defects cause no quenching in sodalime glass. The extrapolated radiative decay rate is 42 s$^{-1}$ (corresponding to $\tau = 24$ ms).

(b) Alkali-borosilicate glass. The increase in PL decay rate with Er density is due to both implantation-induced defects – of which the density depends on fluence – and Er-concentration dependent energy

migration. The energy transfer coefficient is $C_{Er,Er} = 0.86 \times 10^{-51}$ $m^6/s$. Implantation-induced damage causes significant internal non-radiative quenching for each Er ion. This damage production is attributed to the presence of boron in the glass, which increases the sensitivity for ionization damage.

Resonant Er-to-Er energy transfer in borosilicate glass is less efficient than in soda-lime glass, which is partly due to the stronger inhomogeneous broadening of the $4f$ manifolds in borosilicate glass. Therefore, the effect of concentration quenching is lower in borosilicates than in sodalime glass. However, ion implantation is not a suitable technique to dope borosilicates with optically active ions, due to the effect of irradiation damage leading to low luminescence lifetimes. In the design of planar amplifiers, not only concentration quenching due to energy migration, but also cooperative upconversion should be taken into account. In many cases the latter will be the dominant decay process.

## Acknowledgements

It is a pleasure to thank M. Fleuster (KFA Jülich, Germany) for implantations of BGG 31 silicate and discussions. D. Simons (TNO-institute of Applied Physics, Eindhoven, The Netherlands) is acknowledged for IR transmission and reflection measurements. This work is part of the research program of the Foundation for Fundamental Research on Matter (FOM), and was made possible by financial support from the Dutch Organization for the Advancement of Pure Research (NWO), the Netherlands Technology Foundation (STW), and the IC Technology Program (IOP Electro-Optics) of the Ministry of Economic Affairs.

## References

[1] E. Desurvire, Physics Today 47 (1994) 20.
[2] C.H. Henry, G.E. Blonder and R.F. Kazarinov, J. Lightwave Technol. 7 (1989) 1530.
[3] J. Viljanen and M. Leppihalme, Proc. First Europ. Conf. on Integrated Optics (London, Great Britain, 1981) p. 18.
[4] S. Iraj Najafi, Appl. Optics 27 (1988) 3728.
[5] L. Roß, Glastech. Ber. 62 (1989) 285.
[6] W.J. Miniscalco, J. Lightwave Technol. 9 (1991) 234.
[7] J.C. Wright, in: Radiationless processes in Molecules and Condensed Phases, ed. F.K. Fong (Springer, Heidelberg, 1976) Chapter 4.
[8] F. Auzel, in: Radiationless Processes, ed. B. DiBartolo (Plenum, New York, 1980).
[9] H. Scholze, Glass (Springer, Heidelberg, 1990).
[10] Wei-Kan Chu, J.W. Mayer and M.-A. Nicolet, Backscattering Spectrometry (Academic, New York, 1978).
[11] E. Snoeks, G.N. van den Hoven and A. Polman, J. Appl. Phys. 73 (1993) 8179.
[12] S. Hüfner, Optical Spectra of Transparent Rare-Earth Compounds (Academic, New York, 1978).
[13] E. Snoeks, A. Lagendijk and A. Polman, Phys. Rev. Lett. 74 (1995) 2459.
[14] R. Brückner and H. Hessenkemper, Glastech. Ber. 66 (1993) 245.
[15] H. Scholze, Glastech. Ber. 32 (1959) 142.
[16] H. Scholze, Glastech. Ber. 32 (1959) 81.
[17] V.P. Gapontsev, A.A. Izyneev, Yu. E. Sverchov and M.R. Syrtlanov, Sov. J. Quantum Electron. 11 (1981) 1101.
[18] Yingchao Yan, A.J. Faber and H. de Waal, J. Non-Cryst. Solids 181 (1995) 283.
[19] A.J. Bruce, W.A. Reed, A.E. Neeves, L.R. Copeland, W.H. Grodkiewicz and A. Lidgard, Mat. Res. Soc. Symp. Proc. 244 (1992) 157.
[20] Th. Förster, Discuss. Faraday Soc. 27 (1959) 7;
Th. Förster, Ann. Physik 2 (1948) 55.
[21] P.G. de Gennes, J. Phys. Chem. Solids 7 (1958) 345.
[22] M.J. Weber, Phys. Rev. B 4 (1971) 2932.
[23] N. Krasutsky and H.W. Moos, Phys. Rev. B 8 (1979) 1010.
[24] J.P. Biersack and L.J. Haggmark, Nucl. Instrum. Methods 174 (1980) 257.
[25] F. Caccavale, G. de Marchi, P. Mazzoldi, C. Meneghini, A. Quaranta, G.W. Arnold, G. Battaglin and G. Mattei, Nucl. Instrum. Methods B96 (1995) 382.
[26] R.H. Magruder III, Li Yang, R.F. Haglund, Jr., C.W. White, Lina Yang, R. Dorsinville and R.R. Alfano, Appl. Phys. Lett. 62 (1993) 1730.
[27] A. Perez, M. Treilleux, T. Capra and D.L. Griscom, J. Mater. Res. 2 (1987) 910.
[28] F.F. Morehead, Jr. and B.L. Crowder, Radiat. Eff. 6 (1970) 27.
[29] D.L. Griscom, G.H. Sigel, Jr. and R.J. Ginther, J. Appl. Phys. 47 (1976) 960.
[30] V.P. Gapontsev, S.M. Matitsin, A.A. Izineev and V.B. Kravchenko, Erbium glass lasers and their applications, in: Optics and Laser Techn. 14 (Butterworth, 1992) pp. 189–196.
[31] E. Snoeks, G.N. van den Hoven, A. Polman, B. Hendriksen, M.B.J. Diemeer and F. Priolo, J. Opt. Soc. Am. B 12 (1995) 1468.